Evaluating AFM as an analysis tool for graphene

What is graphene?

Graphene is the most famous member of the 2D materials family: a sheet of covalently bonded carbon atoms in a hexagonal lattice in which the thickness has been reduced to a single atom. This unique nanomaterial is extraordinarily strong and has the highest known thermal and electrical conductivity. It was awarded the Nobel prize for Physics in 2010, for research done by Andre Geim and Konstantin Novoselov.

There are many other 2D materials that are being actively explored. A collective group of graphene-like structures is known as xenes – which are also monolayers of a single element. For example, single layer of black phosphorus, phosphorene, is a promising material for transistors. Other examples are silicene (silicon), germanene (germanium), and stanine (tin), all exhibiting a hexagonal structure like graphene with various degrees of buckling.

Hexagonal boron nitride (h-BN) has the same overall structure as graphene but replaces the carbon atoms with alternating boron and nitrogen atoms. Finally, members of another popular class of 2D materials are transition metal dichalcogenides with the chemical formula MX_2, where M is a transition metal such as tungsten or molybdenum and X is a chalcogen such as Sulphur, selenium, or tellurium.

Interest in stacking of graphene on itself or other 2D materials is currently gaining traction. An angular or lattice mismatch has been shown to create different electrical properties of the layered stack. This opens the door to creating new devices in a bottom-up approach, stacking multiple layers of 2D materials under such angles that allow tuning of the properties. However, as relaxation processes after deposition occur, control measurements are needed to verify the angular mismatch between the layers.

Why AFM?

AFM has become the instrument of choice for studying nanomaterials for two key reasons: resolution, and availability of many different modes enabling comprehensive characterization of a nanomaterial, including its mechanical and electrical properties beyond the topography. The exceptional x-, y-, and z-resolution are important due to phenomena close to the atomic scale. The resolution of a commercial AFM ranges from less than a few nanometers all the way to atomic resolution laterally, and better than 0.1 nm vertically. This makes AFM one of the few types of instruments that can attain the resolution required to measure nanosheets that are only a few angstroms thick.

Another advantage of AFM that has real-life implications is the available suite of measurement modes to assess electrical and mechanical properties simultaneously to the topography. These modes can be used to study those additional properties in detail, or simply as a contrast mechanism to evaluate the quality of grown graphene or the angular mismatch between stacked layers of graphene. This makes AFM an indispensable tool for device design that relies on the stacking of 2D materials.

Finally, the AFM tip can be used to manipulate samples at the nanoscale. In the

case of graphene, it can, for example, be used to cut through graphene sheets. The two halves of a single graphene sheet cut in two have the same crystal orientation, enhancing the control of the angular mismatch during stacking.

Besides these imaging properties, an additional motivation for utilizing AFM originates from its small footprint, allowing it to be placed inside a glovebox. This is a prerequisite to studying graphene in combination with 2D materials that are sensitive to the presence of oxygen or humidity.

Applications

Examples of the power of AFM to characterize graphene are presented in the following applications.

1. **Flake thickness:** The first example illustrates the superb resolution of AFM. *Figure 1* reveals several stacked layers of graphene oxide, enabling analysis of the thicknesses of the individual layers. A corresponding height histogram of the measurement shows the thinnest layer to be a mere 0.75 nm. This image demonstrates the exceptional vertical resolution of AFM at the level required to study 2D materials.

2. **Graphene growth analysis:** An example of the ability to check the quality of graphene is shown in *Figure 2*. The sample consists of graphene grown by chemical vapor deposition (CVD) on
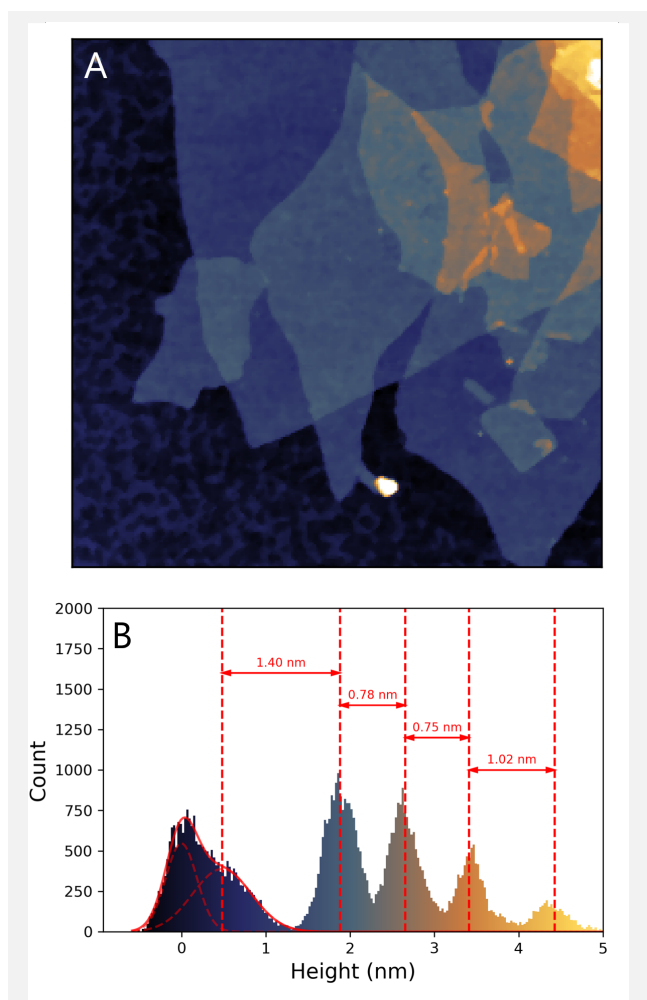

Figure 1. Measuring the thickness of multilayer graphene. (A) AFM topographical image of graphene oxide with lateral dimensions of 5.11 x 5.11 μm^2. (B) Histogram of the heights in (A) showing the thickness of the first 4 layers.
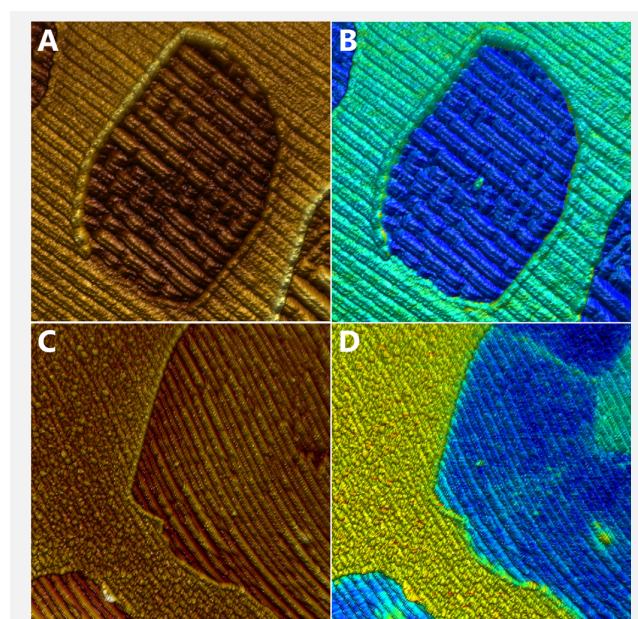Sample courtesy: Nanotech Energy, USA.

Figure 2. Quality control of chemical vapor deposition (CVD) grown graphene on post-oxidized copper by lateral force imaging and KPFM. (A) Topography and (B) friction force images, simultaneously recorded. The friction was calculated from the difference between the forward and backward lateral deflection channels. Scan size: 5 x 5 $\mu m2$. (C) Topography and (D) contact potential difference images. Scan size 10 x 10 $\mu m2$.
Data courtesy: Newtec, A/S Denmark.

nanosurf

copper. The copper substrate is not atomically flat, sometimes obscuring the edges and fine features of the flakes. The copper was oxidized after the deposition, resulting in the height of the oxidized copper exceeding that of the graphene flake in the topography (*Figure* 2A and 2C). The lateral force image (*Figure* 2B) shows a lower friction on the graphene (blue contrast) compared to the copper substrate (green contrast) that assists analysis of the graphene coverage of the copper substrate, since edges have a sharper contrast in the friction channel than in the topography. In addition, the friction image clearly shows a higher friction in the center of the flake, identifying the growth seed point of the flake that is not visible in the topography.

Kelvin probe force microscopy (KPFM) was also used to analyze this sample (*Figure* 2D). Conventionally, KPFM is used to analyze the contact potential difference (CPD) between tip and sample, and under vacuum conditions even the work function. As expected, graphene and the oxidized copper show a different CPD, graphene having a lower value. More importantly, the CPD image shows a heterogeneity on the graphene, with some fine lines and areas on the graphene flakes that are not recognizable in the topography, thus
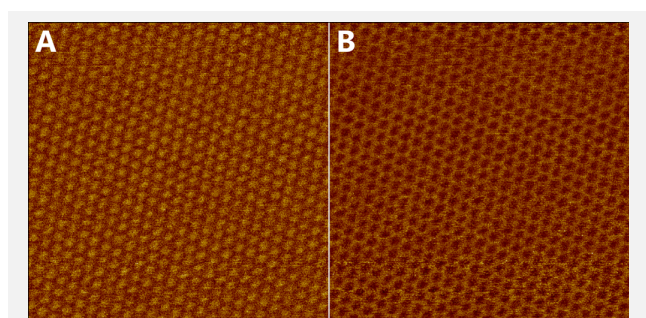

Figure 3: Moiré super lattice of twisted graphene on hBN imaged in PFM mode at the contact resonance frequency. (A) amplitude and (B) phase. Scan size: 154 x 154 nm^2.
Sample courtesy: Nanoelectronics group TIFR, India.

enhancing the quality assessment of the graphene deposition process by AFM.

3. **Lattice mismatch:** The interaction between the AFM tip and a graphene layer also depends on the interaction of the graphene layer with the layer underneath. In the presence of an angular mismatch, the interaction varies periodically with a lattice constant depending on the angular mismatch. This regular pattern, also called moiré super lattice, can be visualized using AFM, for example by piezo-response force microscopy (PFM)[1] or force modulation[2], oscillating the cantilever at the contact resonance frequency. A cantilever with the tip in contact with the sample has different resonances than a free-swinging cantilever. The first contact resonance is very sensitive to the mechanical properties of the sample. The contact resonance can be measured directly with a phase-locked loop or dual frequency resonance tracking, or indirectly but more straightforwardly by detecting the phase and amplitude of the cantilever excited at a fixed frequency on the contact resonance peak. This contact resonance frequency can be determined from a thermal tune spectrum recorded with the tip in contact with the sample.

The angular mismatch between two layers of graphene can be calculated from the periodicity of the moiré superlattice.

Figure 3 shows the phase and amplitude response obtained by imaging a double layer of twisted graphene, clearly displaying the moiré pattern caused by an angular mismatch. The cantilever was electro-statically excited in PFM mode at the contact resonance frequency. Based on the lattice constant of the moiré pattern, the angular mismatch of this sample amounted to 2.2°.

Figure 4 shows the phase response measured in force modulation imaging mode on a DriveAFM[2]. Here, the cantilever was photothermally excited on the contact resonance peak. The 192 nm wide image of *Figure* 4A shows a lattice with some distortion, indicating a variation in the angular mismatch, but still giving multiple diffraction spots in frequency space after
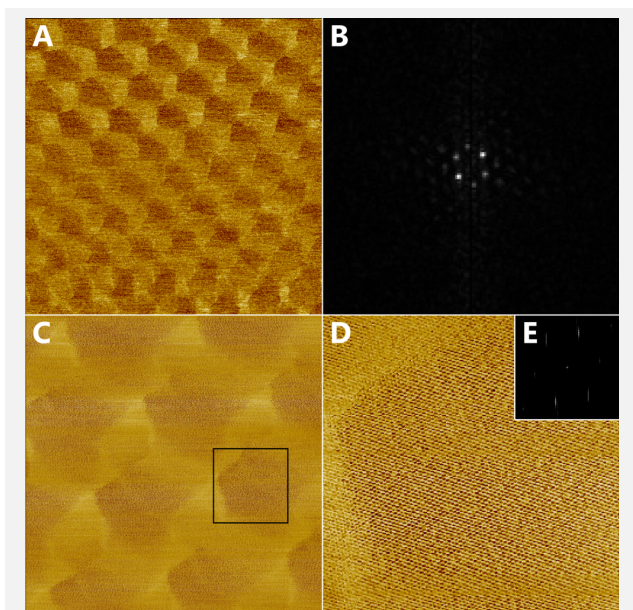

Figure 4: Moiré super lattice of twisted graphene on hBN imaged in force modulation mode on the contact resonance frequency. (A) phase image with scan size of: 190 x 190 nm² (B) Center part of the Fourier transform image used to determine the lattice constant of the moiré pattern (C) phase image of 68 x 68 nm² area rescanned with 1024 x 1024 px² containing both the moiré superlattice and atomic lattice. (D) Digital zoom of the (C). (E) Fourier transform showing the diffraction spots from the atomic lattice.
Sample courtesy: Nanoelectronics group TIFR, India.

Fourier transformation (*Figure* 4B). The frequency of 1/(7.26 nm) of the (2;2) diffraction spot close to the fast scan axis converts to a lattice constant of 29 nm in real space.

This is 117 times larger than the lattice constant of graphene, portraying an angular mismatch close to 0.5°. Recording a 68 nm wide image (C) with 1024 x 1024 px² does not only show the moiré super lattice, but also the atomic lattice. A digital zoom of 17 nm in width of the phase signal is shown in *Figure* 4D, to enhance the visibility of the
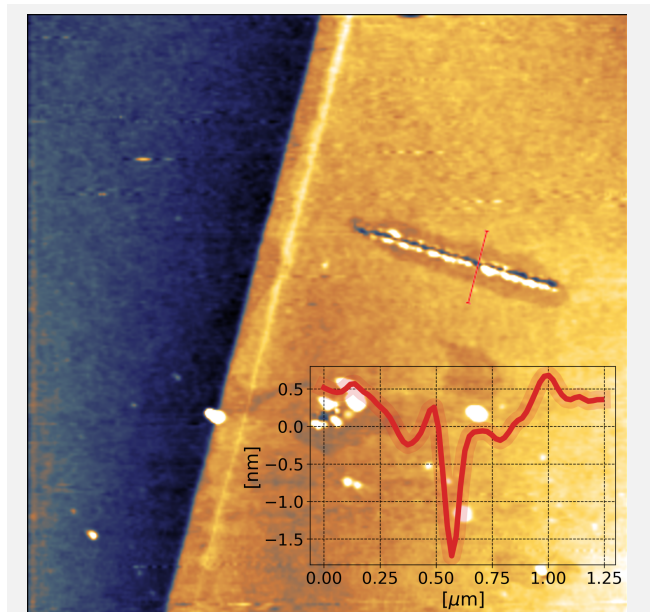

Figure 5: Cutting graphene by AFM lithography. AFM topography image of a multilayer graphene flake on Si substrate with lateral dimensions of 10 x 10 µm². Cuts were obtained by applying a 10V AC voltage at 500 kHz to the tip of a BudgetSensors ElectriTap190E cantilever (k = 48 N/m nominal) and following the designated path in Static Force Mode with an applied force of 5 µN at a speed of 100 nm/s. The relative humidity was 42%.
Sample courtesy: Kim group, Harvard University, USA.

lattice in real space and *Figure* 4F shows the Fourier transform of the phase signal. The atomic lattice was used to verify the lattice of the moiré super lattice.

4. **Cutting graphene:** As mentioned, not only can the AFM tip be used to measure, but also to manipulate materials on the nanometer scale. *Figure* 5 shows an example of a multi-layer stack of graphene that was cut with an AFM tip in nano-lithography mode. The experiment was carried out on a FlexAFM. In lithography, cutting can be controlled by several

parameters, such as force, speed, and direction. At the same time a DC or AC voltage or combination of both can be applied between tip and sample to influence the depth of the cut. It is believed that the cutting mechanism occurs via local anodic oxidation of the surface[3-5]. The high voltages near the tip dissociate H_2O into H and OH groups, which oxidize the graphene. The tip-induced mechanical stress then fractures the graphene at the locations it was oxidized. This is the reason why the relative humidity surrounding the tip plays an important role in graphene cutting. The environmental control add-on allows fine control of the humidity around samples.

Conclusion

Graphene and other 2D materials like xenes – or transition metal dichalcogenides – are a fast-growing topic of interest among leading nanomaterials researchers, with exciting applications in transistors, sensors, and optoelectronics. AFM is uniquely suited to study such materials thanks to its impressive resolution well below a nanometer, capable of clearly showing the atomic lattice and atomic steps. As a multifunctional characterization tool, AFM can measure and correlate multiple important properties of these materials to better understand and characterize them. The detection of moiré patterns is one example of this type of characterization. In addition, AFM can be used to locally manipulate 2D materials.

In summary, this makes AFM indispensable for the study of graphene and other 2D materials in search of ultimate integration into devices and other applications.

References

1. McGilly *et al* 2020 Nat. Nanotechnol. 15, 580–584
2. Adams et al 2021 Rev. Sci. Instr. 92, 129503
3. Puddy *et al* 2011, Appl. Phys. Lett. 98, 133120
4. Masubuchi *et al* 2011, Nano Lett. 11, 4542–4546
5. Li *et al* 2018, Nano Lett. 18, 8011-8015

nanosurf